Manufacturability of CoCrFeNiMnzAlxCuy High Entropy Alloy by Laser Powder Bed Fusion

Eric Barth[(✉)] and Anis Hor

Institut Clément Ader (ICA), Université de Toulouse, CNRS, ISAE-SUPAERO, UPS, INSA, Mines-Albi, 3 Rue Caroline Aigle, 31400 Toulouse, France
{eric.barth,anis.hor}@isae-supaero.fr

Abstract. Six pre-alloyed high entropy alloys powders from the $CoCrFeNiMn_zAl_xCu_y$ family were used to manufacture samples through Laser Powder Bed Fusion technology. These samples were used to assess the manufacturability, microstructure and mechanical properties of the developed alloys. It was found that increasing the Al concentration promoted the formation of a BCC/B2 phase, increasing the hardness and having a direct positive impact on the tensile properties. However, adding more aluminium than what can be found in the $Al_{0.5}CoCrFeNi$ alloy led to extensive manufacturability issues that hindered the tensile properties. On the other hand, the Cu concentration did not appear to yield any significant impact on the microstructures and mechanical properties of the alloys. The considered additively manufactured alloys presented an overall higher hardness than their conventionally manufactured counterparts, but a lower ductility. Thermal treatment led to the precipitation of a σ phase in Al-containing HEAs, and of a secondary FCC phase in Cu-containing alloys. Finally, this paper proves the potential of the $CoCrFeNiAl_x$ alloy family compared to single-phase stainless steels such as 316L and two-phase stainless steels such as SAF 2507.

Keywords: Additive manufacturing · Mechanical properties · microstructure · High entropy alloy

1   Introduction

High Entropy Alloys (HEAs) are a mixture of five or more alloys in equimolar or nearly equimolar proportions [1]. They were first introduced by Cantor et al. [2] in 2004. Since then, these alloys have been extensively studied in the literature [1, 3, 4] as they represent a promising alloying concept for next generation materials. The most studied HEA is the Cantor alloy [2, 5], an equimolar mixture of Co, Cr, Fe, Mn and Ni. However, its properties remain far from being outstanding, as they are close to what can be achieved by a conventional 316L stainless steel [6]. This spurred the publication of various studies aiming at doping the properties of the Cantor alloy by adding new elements [7]. However, these efforts remain limited within the sphere of additively manufactured HEAs.

Additive Manufacturing (AM) presents various characteristics that could greatly enhance the manufacturability and properties of HEAs. Their high-density [1] could

be mitigated by optimized shapes allowed by AM processes. Moreover, it has been found that AM-produced materials exhibit better mechanical properties compared to their conventionally manufactured counterparts [6]. So far, the most commonly used AM technique is Laser Powder Bed Fusion (LPBF), due to its high level of maturity, precision and efficiency.

Cantor alloy, or CoCrFeMnNi alloy was previously manufactured with an LPBF process by Zhu et al. [8]. As with conventional processes, the obtained properties remain similar or lower to what was observed for LPBF conventional alloys made of the same elements. Some efforts were made to further increase the properties of the LPBF-manufactured Cantor alloy by adding Al and Cu in various proportions. It was shown that substituting Mn for various proportions of Al allowed obtaining better hardness and tensile properties due to the precipitation of a hard BCC phase and to the presence of dense dislocation structures [9]. However, going above a critical Al concentration leads to a very brittle behaviour of the alloy and to extensive printability issues, such as cracking due to thermal residual stress [10]. Alternatively, substituting Mn for Cu while remaining equimolar was shown to lead to a highly ductile FCC-phased alloy [11].

2 Materials and Methods

2.1 Powders

CoCrFeMnNi, $Al_{0.3}CoCrFeNi$, $Al_{0.5}CoCrFeNi$, AlCoCrFeNi, AlCuCoCrFeNi and CuCoCrFeNi HEAs were additively manufactured using gas-atomised pre-alloyed powders. The compositions of each powder were analysed by EDX and exhibited the right proportions. The granulometry given by the supplier are 45-90μm for all the powders. The granulometry was also determined using laser diffraction and the obtained results match the values given by the manufacturer. The powders' chemical homogeneity and morphology were analysed using EDX analysis and SEM imaging respectively. All powders present an overall spherical shape, short of a number of satellites and oblong shaped powder grains. Likewise, all powders have good chemical homogeneity, even if some Fe-Rich and Cr-rich grains can be observed in the Al-containing powders.

2.2 Sample Building

Using the aforementioned powders, test samples were built with a SLM 125 HL additive manufacturing machine.

The original plan was to try and apply a single set of building parameters to all the considered alloys, as conducting a parametric optimisation for each alloy proved to be too time-consuming. However, manufacturing issues emerged, and led to a modification of the laser power for each individual alloy. It was then decided to set the hatch distance (h) at 0.1, the layer thickness (t) at 0.05 and the laser velocity at 1000 mm/s (except for Al0.3CoCrFeNi, that used V = 800 mm/s and h = 0.05). The laser power (P) was then varied between 200 W and 300 W until the build-job was able to be successfully completed. The samples were printed both with a vertical and horizontal build-direction, except for Al0.3CoCrFeNi, whose samples were retrieved from a previous build batch where no vertically printed samples were manufactured. The specimens were cut from the baseplate using an Electric Discharge Wire Cutting machine (EDM).

2.3 Heat Treatment

Samples were heat-treated at temperatures of 600 °C, 800 °C and 1100 °C for a duration of 3 h, followed by water-quenching.

2.4 Sample Analysis

The samples' micro-hardness was analysed with a Vickers indent and a 1kg load applied for 20 s. At least 5 measurement per sample orientation were performed. Tensile tests with 6×2.5 mm cross-section specimens (Fig. 1) were performed on an Electromechanical Instron 5900R testing system with at least three tensile tests per build direction and per alloy. Electron backscatter diffraction (EBSD) mappings were performed with a JEOL 7100F SEM. The X-ray diffraction (XRD) measurements for phase characterization were performed with a Bruker's X-Ray diffractometer, using a Cu Kα radiation. The 2θ angle ranged from 28.5° to 105°.
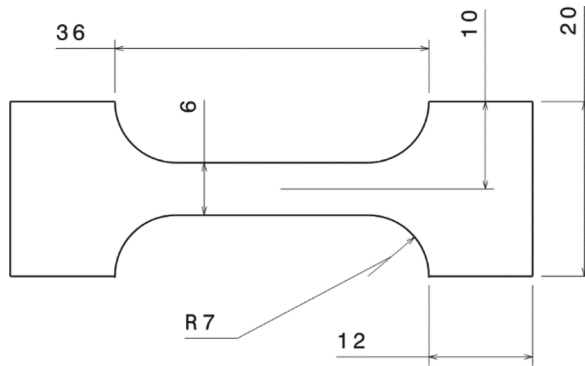
Fig. 1. Blueprint for the used tensile specimens

3 Results

3.1 Chemical Composition

The alloys in this study are composed of elements with melting points ranging from 660 °C for Al to 1857 °C for Co. These differences can complicate the selection of processing parameters, as using a laser power high enough to melt the high melting point elements could evaporate the low-melting point ones. One way of verifying if these parameters are adapted is to check the composition of the sample and compare it with the powder's composition. Here, no major discrepancy was observed. It was noted however that the Al concentration is systematically lower in the sample as it is in the used powder, meaning that a fraction of this element was vaporized during the process.
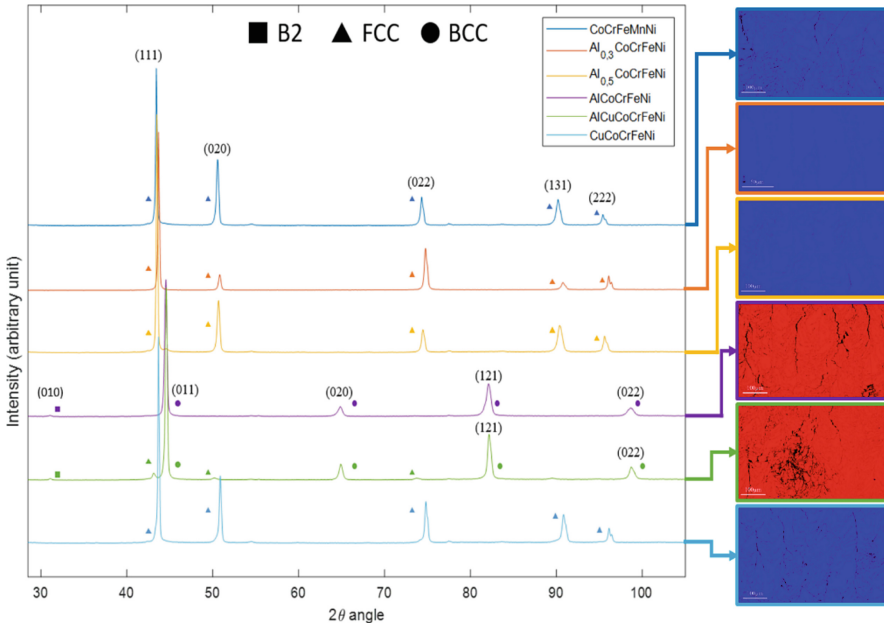
Fig. 2. Results of the XRD phase analysis and corresponding EBSD phase maps for the considered HEA. The BCC phase is represented in red and the FCC phase is represented in blue.

3.2 Samples Structure in the As-Printed State

The phase maps obtained by EBSD analysis of the as-printed samples, as well was the results of the XRD phase analysis are visible in Fig. 2.

We can see that for each sample, the corresponding map is monochromatic, meaning that a single phase was detected per alloy. All alloys are pure FCC, except for AlCoCr-FeNi and AlCuCoCrFeNi, which are pure BCC. However, as visible on the XRD analysis, $Al_{0.5}CoCrFeNi$ and AlCuCoCrFeNi both exhibit a dual-phased composition, with small proportions of BCC and FCC, respectively.

It can be seen that CoCrFeMnNi, $Al_{0.3}CoCrFeNi$ and $Al_{0.5}CoCrFeNi$ present an overall dense structure, with a low concentration of pores and cracks, even without optimized processing parameters. It is to be noted however that the CoCrFeMnNi sample exhibits a high concentration of micro-cracks.

AlCoCrFeNi, AlCuCoCrFeNi and CuCoCrFeNi present a very high concentration of cracks and porosities. These cracks appear to be aligned with the build direction, and mostly located at the centre of melt-pools, propagating along the grain boundaries.

Using the same EBSD analysis, the average grain size was determined. It appeared that AlCoCrFeNi and AlCuCoCrFeNi had the finest microstructure, with an average grain size of 20.3μm and 17.6μm, respectively.

3.3   Mechanical Properties in the As-Printed State

The obtained hardnesses and tensile properties of the HEA samples are summarized in Fig. 3(a). The reference Cantor alloy (CoCrFeMnNi) average hardness was measured to be 226 HV. By removing Mn and increasing the Al concentration to obtain the Al0.5CoCrFeNi alloy leads to a 263 HV micro-hardness, a 16% increase compared to the Cantor reference. Augmenting Al concentration until an equimolar concentration is reached (AlCoCrFeNi) more than doubles the micro-hardness compared to the reference Cantor alloy, with a measured average hardness of 525 HV. Adding Cu in equimolar proportions (AlCuCoCrFeNi) leads to a slightly higher average micro-hardness of 550HV.
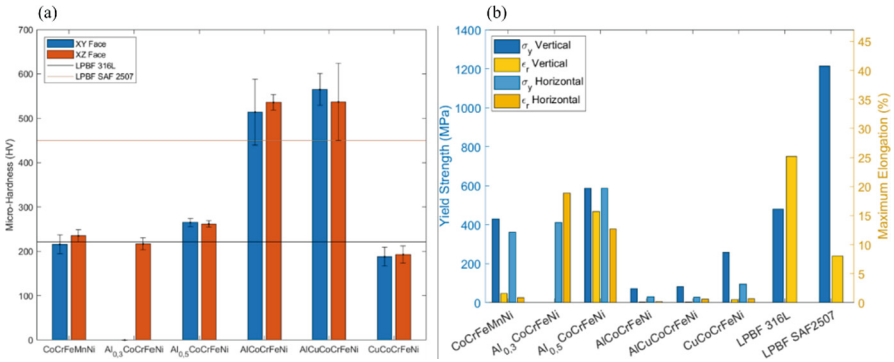

Fig. 3. (a) Microhardness of the samples measured on the XY and XZ faces, with corresponding error bars. The hardnesses of the 316L and SAF 2507 are indicated for comparison purposes. (b) Yield strength elongation at failure of the samples, measured with vertically and horizontally printed samples

By removing Al from the alloy to obtain an equimolar CuCoCrFeNi, we get a measured micro-hardness of 191 HV, a 15% decrease from the reference Cantor alloy.

The tensile tests results of the HEAs are visible on Fig. 3(b). To the exception of Al0.3CoCrFeNi and Al0.5CoCrFeNi, all alloys show a brittle or quasi-brittle tensile behaviour, with very little ductility. Removing Mn and adding Al in the alloy initially increases its tensile strengths, however, going beyond the Al concentration of Al0.5CoCrFeNi leads to a major drop in tensile properties. This is mainly due to the high concentration of pores and microcracks present in the samples. This also applies to AlCuCoCrFeNi. The vertically printed CuCoCrFeNi alloy exhibits a much higher yield and ultimate tensile strength than the horizontally printed ones. However, its tensile performance still remains below the ones of the reference Cantor alloy.

3.4   Effect of Thermal Treatment

The results of the heat-treatment, in terms of observed phases and measured microhardness, are reported in Table 1.

Table 1. Observed phases and microhardness in the AHE samples in the as-printed samples and after heat-treatment at 600 °C, 800 °C and 1100 °C for 3h followed by water-quenching

Alloy		As-printed	600 °C 3h	800 °C 3h	1100 °C 3h
CoCrFeMnNi	Observed phases	FCC	FCC	FCC	FCC
	μhardness (HV1)	226	248	229	212
Al$_{0.5}$CoCrFeNi	Observed phases	FCC + BCC	FCC + BCC	FCC + BCC + σ	FCC + BCC
	μhardness (HV1)	273	355	417	266
AlCoCrFeNi	Observed phases	BCC	BCC	BCC + FCC + σ	BCC + FCC
	μhardness (HV1)	465	545	492	318
AlCuCoCrFeNi	Observed phases	BCC + FCC	BCC + FCC	FCC + BCC + FCC2 + σ	FCC + BCC + FCC2
	μhardness (HV1)	466	473	357	300
CuCoCrFeNi	Observed phases	FCC	FCC + FCC2	FCC + FCC2	FCC + FCC2
	μhardness (HV1)	183	207	197	197

Except for the reference Cantor alloy, multiple new phases appear in all of the AHE. The small amount of BCC and FCC phase observed in Al$_{0.5}$CoCrFeNi and AlCuCoCr-FeNi respectively increases with temperature. A secondary FCC phase appears at higher treatment temperature for the AlCoCrFeNi.

For all Al-containing alloys, a σ phase is observed for the 800 °C heat-treatment, but is absent after the 1100 °C one, giving us thresholds for the precipitation and dissolution temperatures of this phase.

For Cu-containing alloys, a secondary FCC phase with different lattice parameters is observable after the 600 °C treatment for the CuCoCrFeNi alloy and after the 800 °C for the AlCuCoCrFeNi.

All samples exhibit an increase in hardness after the first 600 °C treatment, even AlCuCoCrFeNi, within which the concentration of the soft FCC phase increases. This can be explained by a better dissolution of the various elements in the alloy's lattice, increasing solid solution strengthening [12]. Except for Al$_{0.5}$CoCrFeNi, which hits a hardness maximum after the 800 °C treatment due to the precipitation of the BCC and sigma phase, all alloys' hardness decreases for treatment temperatures beyond 600 °C. These subsequent decrease in the measured microhardness could be explained by grain coarsening [13], but this will have to be verified by further microstructural analysis.

4   Discussion

4.1   Impact of Al and Cu Concentration on the Mechanical Properties

The measured hardness increase with Al concentration was observed before for the AlxCoCrFeNi family obtained through vacuum arc melting and casting, as well as by Laser Metal Deposition method [14]. This behaviour remains visible when an LPBF process is used. Here, this hardness increase can be explained by the transition of the alloy from an FCC phase to a BCC phase, which was already observed for the conventionally alloyed AlxCoCrFeNi family [14]. It can also be explained by the fine granular structure observed for the equimolar AlCoCrFeNi alloy. However, the process induced cracks and pores led to very brittle behaviours and poor tensile properties for AlCoCrFeNi, AlCuCoCrFeNi and CuCoCrFeNi. For the latter, the high crack concentration can be explained by the precipitation of a brittle intergranular Cu-rich phase [15].

AlCoCrFeNi and AlCuCoCrFeNi present similar properties and microstructure. Likewise, there are no significant differences between the properties of CuCoCrFeNi and the properties of the reference Cantor alloy. This suggests that the Al concentration has a much higher impact on the properties of the CoCrFeMnNiAlCu family than the Cu concentration does.

As expected, the hardness obtained for the Cantor alloy is similar to what can be observed for an LPBF 316L stainless steel. Al0.3CoCrFeNi, Al0.5CoCrFeNi and CuCoCrFeNi also have hardness of similar magnitude. However, for the BCC-phase HEA (AlCoCrFeNi and AlCuCoCrFeNi), their hardness is even higher than what can be achieved with an LPBF SAF 2507 Super Duplex alloy, which is also fully BCC after LPBF manufacturing.

4.2   LPBF Induced Phase Repartition

The fast cooling rate inherent to laser fusion processes was shown to hamper the formation of secondary phases in otherwise dual-phase alloys. This can diminish the overall attractivity of these alloys, as their main advantage is to have a good strength/ductility trade-off thanks to their dual FCC/BCC structure. This issue could be solved with one of the thermal treatments applied to the samples, and remains to be verified through proper tensile tests.

5   Discussion

This study analyses the effect of a progressive variations of the Cantor alloy's composition, using multiple different concentrations of Al and/or Cu, on their LPBF printabilities, microstructures and mechanical properties. It led to the following conclusions:

1/ The observed phases in the as-printed state were FCC, BCC/B2 or a combination of both. For the later, only one of the two phases were visible on the EBSD phase maps, this being supposedly due to the extreme cooling speeds inherent to the LPBF process.

2/ Adding Al promotes the formation of a BCC/B2 phase, while also improving the hardness and the tensile properties up until $Al_{0.5}$. Going beyond this Al concentration

leads to a significant degradation in tensile properties due to cracks and pores. Adding Copper does not change the FCC phase observed in the reference Cantor alloy, nor significantly changes the mechanical properties.

3/ Heat treatment leads to the formation of a σ-phase at 800 °C for Al-containing HEAs, which disappears after a 1100 °C treatment. For Cu-containing HEAs, a secondary FCC phase with different lattice parameters appears. Overall, hardness increases after a 600 °C treatment, which can be explained by a better dissolution of the elements in the matrix leading to the increase of solid solution strengthening phenomena.

References

1. Zhang, Y., et al.: Microstructures and properties of high-entropy alloys. Prog. Mater. Sci. **61**, 1–93 (2014). https://doi.org/10.1016/j.pmatsci.2013.10.001
2. Cantor, B., Chang, I.T.H., Knight, P., Vincent, A.J.B.: Microstructural development in equiatomic multicomponent alloys. Mater. Sci. Eng. A **375–377**, 213–218 (2004). https://doi.org/10.1016/j.msea.2003.10.257
3. Zhang, Y., Yang, X., Liaw, P.K.: Alloy design and properties optimization of high-entropy alloys. JOM **64**, 830–838 (2012). https://doi.org/10.1007/s11837-012-0366-5
4. Ye, Y.F., Wang, Q., Lu, J., Liu, C.T., Yang, Y.: High-entropy alloy: challenges and prospects. Mat. Today **19**, 349–362 (2016). https://doi.org/10.1016/j.mattod.2015.11.026
5. Shams, S.A.A., et al.: Low-cycle fatigue properties of CoCrFeMnNi high-entropy alloy compared with its conventional counterparts. Mater. Sci. Eng. A **792**, 139661 (2020). https://doi.org/10.1016/j.msea.2020.139661
6. Bartolomeu, F., et al.: 316L stainless steel mechanical and tribological behavior—A comparison between selective laser melting, hot pressing and conventional casting. Addit. Manuf.. Manuf. **16**, 81–89 (2017). https://doi.org/10.1016/j.addma.2017.05.007
7. Xian, X., et al.: Precipitation and its strengthening of Cu-rich phase in CrMnFeCoNiCux high-entropy alloys. Mat. Sci. Eng. A **713**, 134–140 (2018). https://doi.org/10.1016/j.msea.2017.12.060
8. Zhu, Z.G., et al.: Hierarchical microstructure and strengthening mechanisms of a CoCrFeNiMn high entropy alloy additively manufactured by selective laser melting. Scripta Mater. **154**, 20–24 (2018). https://doi.org/10.1016/j.scriptamat.2018.05.015
9. Zhou, P.F., Xiao, D.H., Wu, Z., Ou, X.Q.: Al0.5FeCoCrNi high entropy alloy prepared by selective laser melting with gas-atomized pre-alloy powders. Mater. Sci. Eng. A **739**, 86–89 (2019). https://doi.org/10.1016/j.msea.2018.10.035
10. Karlsson, D., et al.: Elemental segregation in an AlCoCrFeNi high-entropy alloy – a comparison between selective laser melting and induction melting. J. Alloy. Compd. **784**, 195–203 (2019). https://doi.org/10.1016/j.jallcom.2018.12.267
11. Gao, J., et al.: Fabricating antibacterial CoCrCuFeNi high-entropy alloy via selective laser melting and in-situ alloying. J. Mater. Sci. Technol. **102**, 159–165 (2022). https://doi.org/10.1016/j.jmst.2021.07.002
12. Lee, C., et al.: Lattice distortion in a strong and ductile refractory high-entropy alloy. Acta Mater. **160**, 158–172 (2018). https://doi.org/10.1016/j.actamat.2018.08.053

13. Callister, Jr.: WD Fundamentals of Materials Science and Engineering, 5th edn. John Wiley & Sons, Inc.
14. Wang, W.-R., Wang, W.-L., Wang, S.-C., Tsai, Y.-C., Lai, C.-H., Yeh, J.-W.: Effects of Al addition on the microstructure and mechanical property of AlxCoCrFeNi high-entropy alloys. Interm. **26**, 44–51 (2012). https://doi.org/10.1016/j.intermet.2012.03.005
15. Du, C., Hu, L., Pan, Q., Chen, K., Zhou, P., Wang, G.: Effect of Cu on the strengthening and embrittling of an FeCoNiCr-xCu HEA. Mater. Sci. Eng. AA **832**, 142413 (2022). https://doi.org/10.1016/j.msea.2021.142413